

Numerical analysis and field monitoring tests on shallow tunnels under weak surrounding rock

LIU Jian-hua(刘建华)¹, LIU Xiao-ming(刘晓明)², ZHANG Yong-jie(张永杰)³, XIAO Ting(肖庭)¹

1. School of Traffic and Transportation Engineering, Changsha University of Science and Technology, Changsha 410004, China;

2. College of Civil Engineering, Hunan University, Changsha 410082, China;

3. School of Civil Engineering and Architecture, Changsha University of Science and Technology, Changsha 410004, China

© Central South University Press and Springer-Verlag Berlin Heidelberg 2015

Abstract: The Jianpudong No. 4 tunnel is a shallow tunnel, which belongs to Shaoshan County scenic highway in Hunan province, China and whose surrounding rock is weak. According to its characteristics, the field monitoring tests and numerical analysis were done. The mechanical characteristics of shallow tunnels under weak surrounding rock and the stress–strain rule of surrounding rock and support were analyzed. The numerical analysis results show that the settlement caused by upper bench excavating accounts for 44% of the total settlement, and the settlement caused by tunnel upper bench supporting accounts for 56% of the total settlement. The maximum axial force of shotcrete lining is 177.2 kN, which locates in hance under the secondary lining. The maximum moment of shotcrete lining is 5.08 kN·m, which locates in the arch foot. The stress curve of steel arch has three obvious stages during the tunnel construction. The maximum axial force of steel arch is 297.4 kN, which locates in tunnel vault. The axial forces of steel arch are respectively 23.5 kN and –21.8 kN, which is influenced by eccentric compression of shallow tunnel and locates in hance. The results show that there is larger earth pressure in tunnel vault which is most unfavorable position of steel arch. Therefore, the advance support should be strengthened in tunnel vault during construction process.

Key words: tunnel engineering; shallow tunnel; weak surrounding rock; numerical analysis; field monitoring tests

1 Introduction

More and more tunnels and underground engineering projects have been built in China, because they are fast, safe, reliable, punctual, comfortable, and convenient, also they occupy less land, protect ground landscape, ensure smooth lines, carry lots of passengers rapidly, and reduce ground traffic congestion effectively [1–3].

Unfavorable geologic conditions including shallow buried, soft or weak geology stratum and broken surrounding rock belt, are often met during tunnel construction. There generally are weathering and breakage rock surrounding tunnel, and eccentric compression for tunnel due to the shallow buried depth. Therefore, the stress distribution and deformation of surrounding rock and supporting structure in tunnel are very complicated [4–5]. To overcome these problems, the ground reinforcement and longitudinal tunnel reinforcements must be provided before the tunnel is excavated [6–7].

Especially for shallow buried tunnel construction in greatly undulate hilly terrain regions, the stress distribution of surrounding rock and deformation condition of tunnel lining is more complicated [8–9]. In the excavation process or after construction, the settlement of vault is often prone to increase sharply, the tunnel section deforms to shrink, the earth surface cracks, and even the tunnel construction face collapses sometimes. There are many difficulties in tunnel design stage and more difficulties for deformation and stability control in construction stage which are prone to landslides and other safe accidents [10–11].

Because tunnel supports can be installed only after considerable deformation has occurred, it is not possible to use these supports as a means of preventing deformation before or immediately after the excavation. Furthermore, additional ground disruption caused by the installation of supports is unavoidable [12–13].

However, difficulties in the prediction of tunnel face stability are present in all the currently existing simplified models. There are limitations to control the deformation of the ground with supports inside the

Foundation item: Projects(51408060, 51208063) supported by the National Natural Science Foundation of China

Received date: 2014–10–15; **Accepted date:** 2015–05–15

Corresponding author: LIU Jian-hua; Associate Professor, PhD; Tel: +86–18627577986; E-mail: tomystone@126.com

tunnel based on the numerical analysis and field monitoring for shallow tunnels [14–15]. Therefore, the mechanical characteristics of shallow tunnels under weak surrounding rock and the stress–strain rule of surrounding rock and support were analyzed in this work. According to the characteristics of shallow tunnel under weak surrounding rock, the numerical analysis and field monitoring tests on shallow tunnel under weak surrounding rock were carried out based on Jianpudong No. 4 tunnel project of Shaoshan County scenic highway in Hunan province, China.

2 Numerical modeling of shallow tunnel

The Jianpudong No. 4 tunnel project of Shaoshan County scenic highway in Hunan province, China locates in the west of the former residence of Chairman Mao by 800 m. The stratigraphical distribution of that project includes two epochs of stratum, Quaternary strata, upper of Devonian, etc. The Quaternary strata is mainly clay and gravelly soil in the mountain depression with 1–4 m in thickness. The Pleistocene series of Quaternary strata are mostly distributed in hillsides and slopes.

2.1 Numerical modeling of tunnel support

The finite element method is used to establish the numerical model. The plane strain quadrilateral element or solid element is adopted to simulate the tunnel surrounding rock and the first lining which is assumed as continuum. Beam elements are adopted to simulate initial support and implantable truss elements are adopted to simulate anchor bolt [16].

2.1.1 Beam element

The beam element consists of two nodes, which has tensile strength, shear strength, flexural rigidity and torsional rigidity, as shown in Fig. 1.

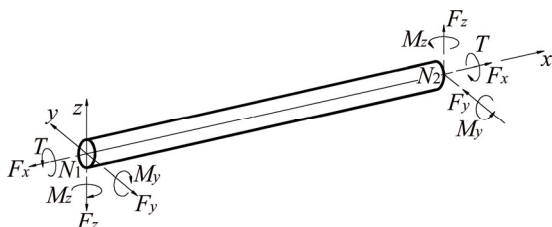


Fig. 1 Internal forces of beam element

The displacements of the beam element are as follows:

$$u = z\beta_y(x), \quad w = w(x) \tag{1}$$

where u is the displacement along x direction, w is the displacement along z direction, and β_y is the rotation displacement along the y -axis.

The strain and curvature are as follows:

$$\varepsilon_b = \varepsilon_x = \frac{\partial u}{\partial x} = z \frac{\partial \beta_y}{\partial x} = z\kappa_y \tag{2}$$

$$\gamma_s = \gamma_{xz} = \frac{\partial w}{\partial x} + \beta_y \tag{3}$$

where ε_b is the flexural strain, γ_s is the shear strain, and κ_y is the curvature along the y -axis.

The relationships of moment and curvature, shear and shear strain are as follows:

$$M_y = D_b \kappa_y = EI \frac{\partial \beta_y}{\partial x} \tag{4}$$

$$V_y = D_s \bar{\gamma}_{xz} = GA_s \bar{\gamma}_{xz} \tag{5}$$

where D_b is flexural stiffness, D_s is shear stiffness, E is elasticity modulus, I is inertial moment, G is shear modulus and A_s is shear area.

The shape function of rotation displacement between two nodes of beam element is

$$\beta_y = N_1 \beta_{y1} + N_2 \beta_{y2} + N_3 \Delta \beta_{y3} \tag{6}$$

$$N_1 = \frac{1-\xi}{2}, \quad N_2 = \frac{1+\xi}{2}, \quad N_3 = 1-\xi^2 \tag{7}$$

The curvature is calculated according to the shape function above as follows:

$$\begin{aligned} \kappa_y &= \frac{\partial N_1}{\partial x} \beta_{y1} + \frac{\partial N_2}{\partial x} \beta_{y2} + \frac{\partial N_3}{\partial x} \Delta \beta_{y3} \\ &= J^{-1} \left(\frac{\partial N_1}{\partial \xi} \beta_{y1} + \frac{\partial N_2}{\partial \xi} \beta_{y2} + \frac{\partial N_3}{\partial \xi} \Delta \beta_{y3} \right) \\ &= J^{-1} \begin{bmatrix} 0 & \frac{\partial N_1}{\partial \xi} & 0 & \frac{\partial N_2}{\partial \xi} \end{bmatrix} \begin{Bmatrix} w_1 \\ \beta_{y1} \\ w_2 \\ \beta_{y2} \end{Bmatrix} + J^{-1} \frac{\partial N_3}{\partial \xi} \Delta \beta_{y3} \\ &= \mathbf{B}_{b\beta} u + \mathbf{B}_{b\Delta\beta} \Delta \beta_{y3} \end{aligned} \tag{8}$$

where J is Jacobi factor, and $J = \frac{\partial x}{\partial \xi} = \frac{l}{2}$.

Furthermore, the formula of shear strain is

$$\bar{\gamma}_{xz} = \frac{V_y}{D_s} = \frac{1}{D_s} \frac{\partial M_y}{\partial x} = \frac{D_b}{D_s} \frac{\partial^2 \beta_y}{\partial x^2} \tag{9}$$

The quadratic equation for rotation angle β_y is expressed as

$$\beta_y = \left(1 - \frac{x}{l}\right) \beta_{y1} + \frac{x}{l} \beta_{y2} + 4 \frac{x}{l} \left(1 - \frac{x}{l}\right) \Delta \beta_{y3} \tag{10}$$

The shear strain formula is as follows:

$$\bar{\gamma}_{xz} = B_{s\Delta\beta} \Delta \beta_{y3} = -\frac{2}{3} \phi_3 \Delta \beta_{y3} \tag{11}$$

$$\phi_3 = \frac{D_b}{D_s} \frac{12}{l^2} = \frac{12EI}{GA_s l^2} \tag{12}$$

The shear strain should satisfy the following conditions:

$$\int_0^l (\gamma_{xz} - \bar{\gamma}_{xz}) dx = 0 \tag{13}$$

The above formula is expressed as

$$w_2 - w_1 + \frac{l}{2}\beta_{y1} + \frac{l}{2}\beta_{y2} + \frac{2}{3}l(1 + \phi_3)\Delta\beta_{y3} = 0 \tag{14}$$

The rotation angle equation for beam element nodes is

$$\Delta\beta_{y3} = \mathbf{A}u = \frac{1}{\frac{2}{3}l(1 + \phi_3)} \begin{bmatrix} 1 & -\frac{l}{2} & -1 & -\frac{l}{2} \end{bmatrix} \begin{Bmatrix} w_1 \\ \beta_{y1} \\ w_2 \\ \beta_{y2} \end{Bmatrix} \tag{15}$$

where

$$\mathbf{A} = \mathbf{A}_{\Delta\beta}^{-1} \mathbf{A}_w \tag{16}$$

$$\begin{cases} \mathbf{A}_{\Delta\beta} = \frac{2}{3}l(1 + \phi_3) \\ \mathbf{A}_w = \begin{bmatrix} 1 & -\frac{l}{2} & -1 & -\frac{l}{2} \end{bmatrix} \end{cases} \tag{17}$$

The curvature formula and shear strain formula respectively are

$$\kappa_y = \mathbf{B}_{b\beta}u + \mathbf{B}_{b\Delta\beta}\mathbf{A}u = (\mathbf{B}_{b\beta} + \mathbf{B}_{b\Delta\beta}\mathbf{A})u = \mathbf{B}_b u \tag{18}$$

$$\bar{\gamma}_{xz} = \mathbf{B}_{s\Delta\beta}\mathbf{A}u = (\mathbf{B}_{s\Delta\beta}\mathbf{A})u = \mathbf{B}_s u \tag{19}$$

where \mathbf{B}_b is the relationship matrix between curvature and displacement, and \mathbf{B}_s is relationship matrix between shear strain and displacement.

The stiffness equations are as follows:

$$\mathbf{K} = \mathbf{K}_b + \mathbf{K}_s \tag{20}$$

$$\begin{cases} \mathbf{K}_b = \int_0^l \mathbf{B}_b^T D_b \mathbf{B}_b dx \\ \mathbf{K}_s = \int_0^l \mathbf{B}_s^T D_s \mathbf{B}_s dx \end{cases} \tag{21}$$

2.1.2 Plane strain quadrilateral element

Plane strain element includes triangles and quadrilaterals. In the calculation model, the plane strain quadrilateral element is adopted to simulate rock and soil. There are compressive stiffness, tensile stiffness and shearing stiffness in the plane strain quadrilateral element and compressive stiffness, tensile stiffness on thickness direction. The balance equation of plane strain quadrilateral element is

$$t \int_A \mathbf{B}^T D \mathbf{B} dA u = bt \int_A \mathbf{N}^T dA + pt \int_L \mathbf{N}^T dL + \mathbf{P}_n \tag{22}$$

where L is element length, and t is element thickness whose value is 1.

The numerical integration formula for plane strain

element is

$$t \int_A \mathbf{B}^T D \mathbf{B} dA \longrightarrow t \sum_{j=1}^n \mathbf{B}_j^T D_j \mathbf{B}_j |J_j| W_{1j} W_{2j} \tag{23}$$

where W_{1j} is weights for integration points on ξ direction, and W_{2j} is weight for integration points on η direction.

2.1.3 Implantable truss element

Implantable truss element consists of two nodes and belongs to “uniaxial tension–compression three-dimensional linear unit”, which only transfer axial tension and pressure, and is used to simulate bolt and support.

When the uniaxial deformation for implantable truss element with uniaxial stiffness EA and length l occurs, the formula for deformation energy Π is

$$\Pi = \int_0^l \frac{EA}{2} \left(\frac{du}{dx} \right)^2 dx \tag{24}$$

where u is the uniaxial displacement.

The uniaxial displacement of implantable truss element represented by shape functions and nodal displacement is given as

$$\mathbf{u} = \sum_{i=1}^n N_i \mathbf{u}_i \tag{25}$$

where n is the number of nodes whose value is 2,

$$N_1 = \frac{1}{2}(1 - \xi), \text{ and } N_2 = \frac{1}{2}(1 + \xi) \quad (-1 \leq \xi \leq 1).$$

The strain formula is as follows:

$$\frac{d\mathbf{u}}{dx} = \sum_{i=1}^n \frac{dN_i}{dx} \mathbf{u}_i = \begin{bmatrix} \frac{dN_1}{dx} & \frac{dN_2}{dx} \end{bmatrix} \begin{Bmatrix} u_1 \\ u_2 \end{Bmatrix} \tag{26}$$

The formula for shape function which differential for x is

$$\frac{dN_i}{dx} = \frac{d\xi}{dx} \frac{dN_i}{d\xi} = \mathbf{J}^{-1} \frac{dN_i}{d\xi} \tag{27}$$

The above formula is also expressed as

$$\frac{d\mathbf{u}}{dx} = \mathbf{J}^{-1} \begin{bmatrix} \frac{dN_1}{d\xi} & \frac{dN_2}{d\xi} \end{bmatrix} \begin{Bmatrix} u_1 \\ u_2 \end{Bmatrix} = \mathbf{J}^{-1} \mathbf{B} \mathbf{u} \tag{28}$$

where \mathbf{B} is the strain matrix of implantable truss element.

Substituting Eq. (28) into Eq. (24) obtains that

$$\Pi = \int_0^l \mathbf{u}^T \mathbf{B}^T D \mathbf{B} \mathbf{u} dx = \int_{-1}^1 \mathbf{u}^T \mathbf{B}^T D \mathbf{B} \mathbf{u} J d\xi \tag{29}$$

where D is the uniaxial stiffness of implantable truss element.

The stiffness matrix of implantable truss element is

$$\mathbf{K} = \int_{-1}^1 \mathbf{B}^T D \mathbf{B} J^{-1} d\xi \tag{30}$$

The integral formula is replaced by algebraic equations and expressed as follows

$$K = \frac{EA}{l} \begin{bmatrix} 1 & -1 \\ -1 & 1 \end{bmatrix} \quad (31)$$

The stiffness equation coordinates is element coordinates and stiffness matrix is transformed using other coordinates.

2.2 Numerical model of shallow tunnel

2.2.1 Failure criterion

Considering plastic deformation of surrounding rock in excavation process, Mohr-Coulomb criterion is adopted, and linearly elastic constitutive relationship is adopted for other structural elements.

2.2.2 Initial ground stress field

The value of the initial ground stress field is very critical for the numerical analysis of tunnel construction. For shallow tunnel, the analysis region for tunnel section near earth’s surface and tectonic ground stress is fully eliminated. Therefore, only geostatic stress is considered and tectonic stress is not considered in numerical simulation [17].

2.2.3 Parameter of rock and soil

Based on geological survey report of Jianpudong No. 4 tunnel and “code for design of road tunnel” [18], the physical and mechanical parameters of soil layers are listed in Table 1.

Construction steps of numerical calculation are shown in Fig. 2. The construction steps are as follows: 1) excavation of upper bench; 2) shotcrete and bolt after upper bench construction; 3) excavation of lower bench; 4) shotcrete and bolt after lower bench construction; 5) the secondary lining.

3 Numerical analysis of shallow tunnel

3.1 Displacement of tunnel

The vertical displacement nephograms of the weak surrounding rock under each construction step in double bench tunneling method are shown in Fig. 3.

The displacement of stratum mainly occurs near the construction site. The maximum settlement region is vault position and there is some uplift in the floor of tunnel.

When the whole construction process is finished, the settlement contour lines of each stratum are symmetrical. The maximum settlements caused by each construction step all appear at tunnel section central axis.

The vertical displacement of stratum decreases with the increase of distance from the excavation site. The more the stratum approaches the excavation section, the more displacement isoline densely appears where the main influence region is in the distance of 1–1.5 times of the tunnel diameter.

The main settlement region and settlement volume of stratum increase with construction promoting of shallow tunnels. The maximum earth’s surface settlement occurs in tunnel upper bench excavation process. The lower bench excavation and supporting process has a little influence on the earth’s surface settlement. When the lower bench supporting process is completed, the settlement of stratum has almost finished.

The results of the tunnel vault settlement in each construction step are shown in Fig. 4. The main reason for tunnel vault settlement is tunnel upper bench excavation. When the lower bench support has been completed, the settlement of stratum has almost finished.

3.2 Shotcrete lining

Figure 5 illustrates the axial force and Fig. 6 illustrates the moment for shotcrete lining in each construction step.

During each construction step, the axial force and moment for shotcrete lining have symmetrical distribution. The minimum axial force occurs in vault and the maximum axial force occurs in hance. The maximum moment occurs in arch foot and the minimum moment occurs in hance.

During the whole construction process, the maximum axial force for shotcrete lining is 177.2 kN which locates in hance at construction step 5) and the maximum moment for shotcrete lining is 5.08 kN·m which locates in arch foot at excavation finished.

The axial force and moment have significant mutation in arch foot and boundary position between upper bench and lower bench. Therefore, construction

Table 1 Physical and mechanical parameters of Jianpudong No. 4 tunnel

Material	Thickness, <i>h</i> /m	Length, <i>l</i> /m	Elastic modulus, <i>E</i> /MPa	Poisson ratio, μ	Density, γ /(kN·m ⁻³)	Cohesion, <i>c</i> /kPa	Friction angle, φ /(°)	Lateral pressure coefficient, <i>e</i>
Rock	—	—	1000	0.45	20	50	20	0.5
Reinforcement layer	—	—	1300	0.45	20	65	26	0.5
Shotcrete lining	0.26	—	21000	0.25	23	—	—	—
Bolt	—	3.5(5)	210000	0.3	78.5	—	—	—
Secondary lining	0.5	—	29500	0.18	25	—	—	—

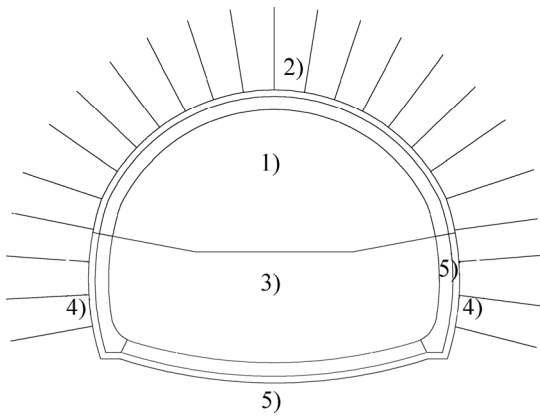


Fig. 2 Construction steps of numerical calculation

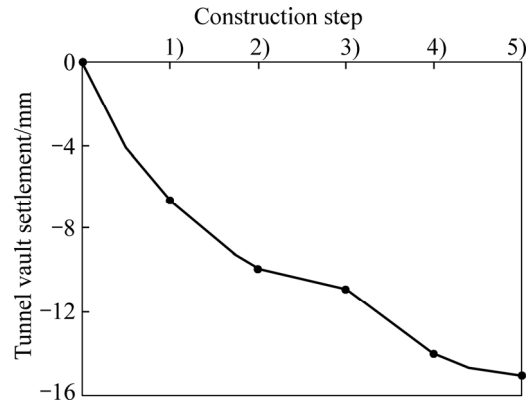


Fig. 4 Tunnel vault settlement in each construction step

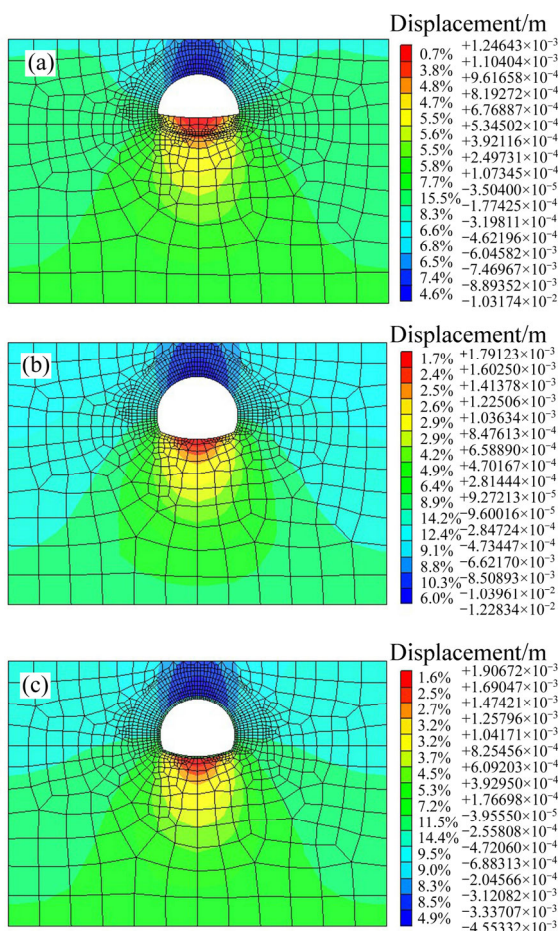


Fig. 3 Vertical displacement nephograms of weak surrounding rock under secondary lining: (a) Excavation of upper bench; (b) Excavation of lower bench; (c) Secondary lining

quality for bolt in these sites must be ensured, and shotcrete lining should be thickened especially in the arch foot.

Figures 7 to 9 respectively illustrate the axial force of bolt in the each construction step.

1) During each construction step, the axial force of bolt generally is below 10 kN.

2) During each construction step, the axial force of bolt is generally smaller in vault than that in

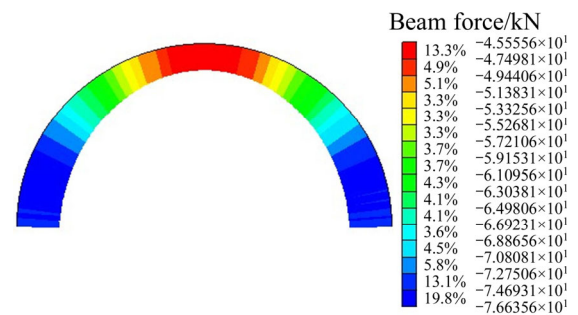


Fig. 5 Axial force for shotcrete lining

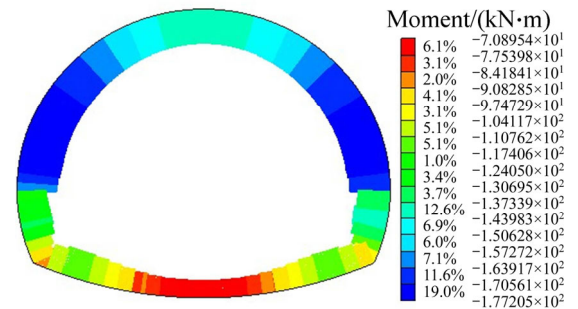


Fig. 6 Moment for shotcrete lining

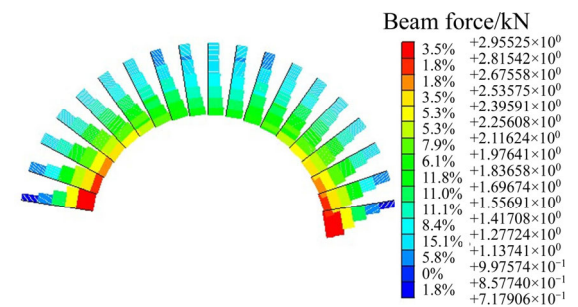


Fig. 7 Axial force of bolt on upper bench construction

two sides of the tunnel. The main reason is that tunnel loose circle has already penetrated to the earth's surface with thin overburden and little hanging reinforcement effect of bolt.

3) The upper bench excavation has a little influence on the axial force of bolt on arch which increases with tunnel excavation and increases by 2 times in tunnel

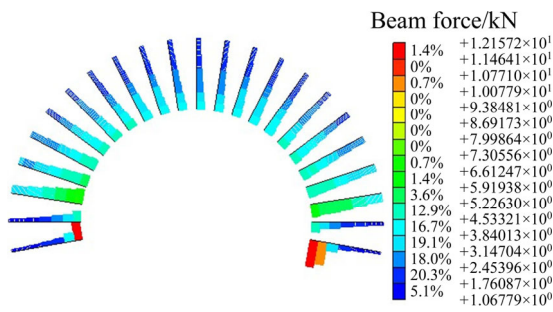


Fig. 8 Axial force of bolt on lower bench construction

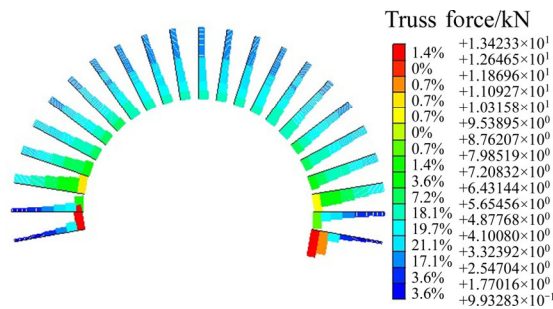


Fig. 9 Axial force of bolt on secondary lining construction

lower bench excavation process. The maximum bolt axial force occurs in arch foot of the tunnel and the value is 1.34 kN.

When the left tunnel construction has been finished, the minimum principal stress of secondary lining for right tunnel is shown in Fig. 10.

Most of the secondary lining is in compression and the maximum compressive stress of secondary lining is 92.3 kPa which is less than the allowable design stress of concrete. The stress concentration of secondary lining is obviously near arch foot of the tunnel and the tension stress region appears with maximum value of only 9.60 kPa. Overall, it is safe for tunnel construction.

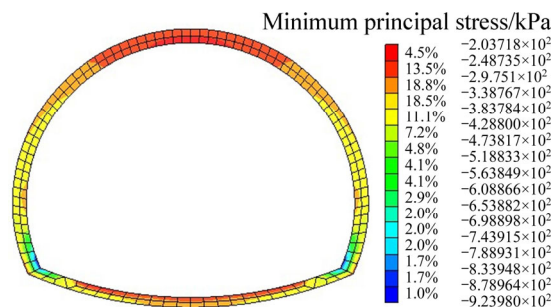


Fig. 10 Minimum principal stress of secondary lining for right tunnel

4 Field monitor test for force of shallow tunnel

According to the specific requirement of NATM and the engineering geology condition of Jianpudong No. 4 tunnel project of Shaoshan County scenic highway in Hunan province, China, the field monitor test includes

visual observation, measurement of convergence displacement, settlement of vault, steel support stress, and the secondary lining internal force and advance geological forecast. Monitoring data consisting of the steel support force and contact pressure between surrounding rock and lining are studied.

4.1 Internal force analysis of steel arch

Figure 11 illustrates the stress variation of steel arch over time. The data curve of stress value has been shaped in three stages over time.

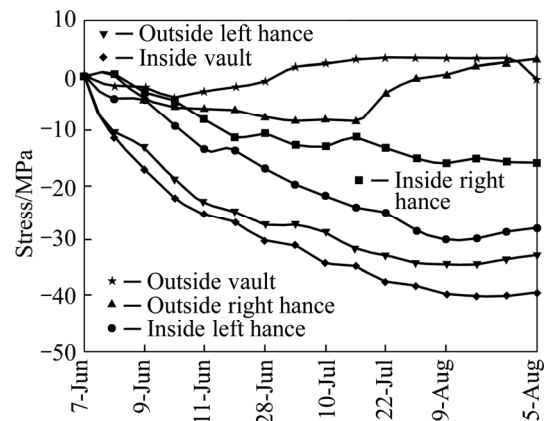


Fig. 11 Stress variation of steel arch over time

The first stage is approximately four days after tunnel upper bench excavating of monitoring section (the distance between tunnel face and monitoring section is 8 m), where the internal force of steel arch increases linearly. At the end of the first stage, internal force value has reached 60%–70% of the final stable value. The second stage is the period after tunnel lower bench excavating and before the construction of inverted arch. The growth rate of steel arch internal force has decreased during this period. At the end of the second stage, internal force value has reached more than 80% of final stable value after tunnel upper bench excavating.

The third stage is the period from the construction of inverted arch to tunnel second lining completed. In this stage, the variation of steel arch internal force becomes stable gradually and the interaction of the structure and surrounding rock tends to be stable.

Figure 12 illustrates the measured axial force distribution of steel arch in K0+784 monitoring section. The maximum axial force for steel arch is 297.4 kN which locates in tunnel vault, and the axial forces of two measuring points are respectively 23.5 kN and –21.8 kN which are influenced by eccentric compression of shallow tunnel and locate in hance. It is shown that there is larger earth pressure in tunnel vault which is most unfavorable position of steel arch.

Figure 13 illustrates the measured moment distribution of steel arch in K0+784 monitoring section.

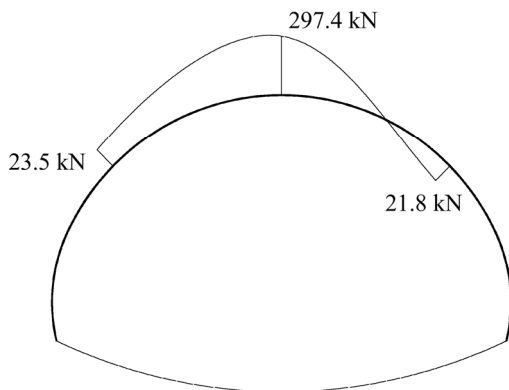


Fig. 12 Measured axial force distribution of steel arch in K0+784 monitoring section

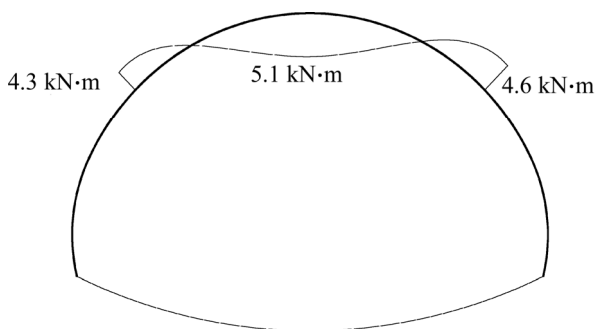


Fig. 13 Measured moment of steel arch in K0+784 monitoring section

The steel arch bears small moment with symmetrical distribution.

4.2 Analysis on contact pressure between surrounding rock and lining

The contact pressure variation over time between surrounding rock and lining is shown in Fig. 14.

The contact pressure between surrounding rock and lining increases rapidly in the initial buried stage. But the growth rate for pressure is reduced over time and tends to be stable with the time increasing.

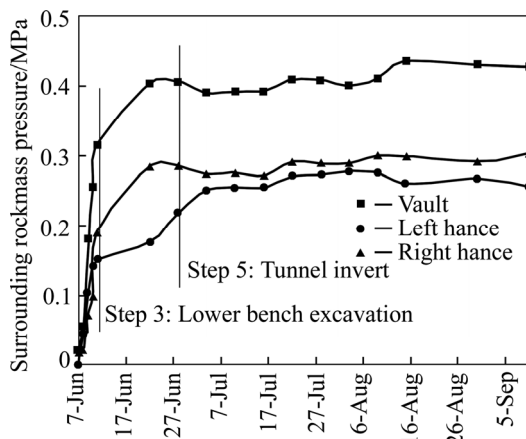


Fig. 14 Contact pressure variation over time between surrounding rock and lining

At the initial stage, affected by the initial stress and construction condition, the field monitoring data are not absolutely actual pressures for surrounding rock but can reflect the changing trends of the pressure between surrounding rock and lining. Once the construction of early supports begins, the pressure increases sharply. Force transmission of supports becomes uniformly with early supports playing a role. In addition, the release rate of surrounding rock stress becomes slow and stress variation of pressure cell becomes small to be stable. When the main excavation and support of tunnel are completed, co-deformation for initial lining and surrounding rock slows down and stabilizes gradually.

The lower bench construction has influence on the pressure of surrounding rock in upper half-section of tunnel where the pressure of surrounding rock obviously changes. The stress state of tunnel structure is improved after the construction of inverted arch is finished and the supporting action of inverted arch is obvious. The construction of inverted arch must be carried out timely.

From the pressure distribution of surrounding rock, there is obviously higher pressure in tunnel vault than in hance. Under the shallow buried condition for tunnel, tunnel vault is the most unfavorable position. Therefore, pre-supporting measures including advance small pipe grouting should be taken to ensure the security of tunnel construction.

5 Conclusions

According to the features of weak surrounding rock and shallow buried tunnel, the numerical analysis and field monitoring tests on shallow tunnel under weak surrounding rock are carried out based on the Jianpudong No. 4 tunnel project of Shaoshan County scenic highway in Hunan province, China. The mechanical characteristics of shallow tunnels under weak surrounding rock and the stress-strain rule of surrounding rock and support are analyzed.

1) The maximum earth’s surface settlement occurs in upper bench excavation process. The lower bench excavation and support have a little influence on settlement. The settlement by tunnel upper bench excavating accounts for 44% of the total settlement and the settlement by tunnel upper bench supporting accounts for 56% of the total settlement.

2) The maximum axial force for shotcrete lining is 177.2 kN which locates in hance under the secondary lining. The maximum moment for shotcrete lining is 5.08 kN·m which locates in arch foot under excavation finished. The axial force and moment have significant mutation in arch foot and boundary position between upper bench and lower bench.

3) The stress curve of steel arch over time has three

stages: sharply increasing, slowly increasing, and then flatten forming. The maximum axial force for steel arch is 297.4 kN which locates in tunnel vault, and the axial forces of two measuring points are respectively 23.5 kN and -21.8 kN influenced by eccentric compression of shallow tunnel and locate in hance. It is shown that there is larger earth pressure in tunnel vault which is the most unfavorable position of steel arch.

4) There is obviously higher pressure in tunnel vault than in hance. Under the shallow buried condition for tunnel, tunnel vault is the most unfavorable position. Therefore, pre-supporting measures including advance small pipe grouting should be taken to ensure the security of tunnel construction.

References

- [1] QIN Chang-bin, SUN Zhi-bin, LIANG Qiao. Limit analysis of roof collapse in tunnels under seepage forces condition with three-dimensional failure mechanism [J]. *Journal of Central South University*, 2013, 20(8): 2314–2322.
- [2] ZHOU Biao, XIE Xiong-yao, YANG Yeong-bin, JIANG Jing-cai. A novel vibration-based structure health monitoring approach for the shallow buried tunnel [J]. *Computer Modeling in Engineering & Sciences*, 2012, 86(4): 321–348
- [3] MOLLON G, DIAS D, SOUBRA A H. Rotational failure mechanisms for the face stability analysis of tunnels driven by a pressurized shield [J]. *International Journal for Numerical and Analytical Methods in Geomechanics*, 2011, 35(12): 1363–1388.
- [4] LAI Hong-peng, XU Xue-shen, CHANU Rui-cheng, XIE Yong-li. Study on mechanical characteristics of highway tunnel expansion [J]. *China Journal of Highway and Transport*, 2014, 27(1): 84–93. (in Chinese)
- [5] KONTOGIANNI V, STIROS S. Convergence in weak rock tunnels [J]. *Tunnels and Tunneling International*, 2006, 38(2): 36–39.
- [6] POPOV N A, KRASYUK A M, LUGIN I V, PAVLOV S A, ZEDGENIZOV D V. Improvement of shallow subway tunnel ventilation procedures [J]. *Journal of Mining Science*, 2015, 50(5): 943–952
- [7] ORESTE P P, DIAS D. Stabilisation of the excavation face in shallow tunnels using fibreglass dowels [J]. *Rock Mechanics and Rock Engineering*, 2012, 45(4): 499–517
- [8] YANG Jun-sheng, ZHANG Jian, YANG Feng. Stability analysis of shallow tunnel face using two-dimensional finite element upper bound solution with mesh adaptation [J]. *Yantu Lixue/Rock and Soil Mechanics*, 2015, 36(1): 257–264. (in Chinese)
- [9] DUAN Bao-fu, ZHU Ying-lei, WU Sheng-zhi. Monitoring and controlling technology for blasting vibration induced by a shallow-buried tunnel in a complex environment [J]. *Modern Tunnelling Technology*, 2013, 50(3): 142–146. (in Chinese)
- [10] KUN M, ONARGAN T. Influence of the fault zone in shallow tunneling: A case study of izmir metro tunnel [J]. *Tunnelling and Underground Space Technology*, 2013, (33): 34–45
- [11] ZHOU Zong-qing, LI Shu-cai, LI Li-ping, SUI Bin, SHI Shao-shuai, ZHANG Qian-qing. Causes of geological hazards and risk control of collapse in shallow tunnels [J]. *Yantu Lixue/Rock and Soil Mechanics*, 2013, 34(5): 1375–1382. (in Chinese)
- [12] POPOV N A, KRASYUK A M, LUGIN I V, PAVLOV S A, ZEDGENIZOV D V. Improvement of shallow subway tunnel ventilation procedures [J]. *Journal of Mining Science*, 2015, 50(5): 943–952
- [13] IBRAHIM O. A new approach for estimating the transverse surface settlement curve for twin tunnels in shallow and soft soils [J]. *Environmental Earth Sciences*, 2014, 72(7): 2357–2367.
- [14] SEO D H, LEE T H, KIM D R, SHIN J H. Pre-nailing support for shallow soft-ground tunneling [J]. *Tunnelling and Underground Space Technology*, 2014, 42: 216–226
- [15] IBRAHIM O. Interaction of longitudinal surface settlements for twin tunnels in shallow and soft soils: The case of istanbul metro [J]. *Environmental Earth Sciences*, 2013, 69(5):1673–1683.
- [16] FRALDI M, GUARRACINO F. Evaluation of impending collapse in circular tunnels by analytical and numerical approaches [J]. *Tunnelling and Underground Space Technology*. 2011, 26(4): 507–516.
- [17] ZHAO Yu, PENG Hai-you, LU Yi-yu. Study on nonlinear dynamic character of interaction between surrounding rock and support structure of deep buried tunnel [J]. *Journal of Highway and Transportation Research and Development*, 2009, 26(11): 98–102. (in Chinese)
- [18] JTJ D70-2004. Code for design of road tunnel [S]. 2004. (in Chinese)

(Edited by FANG Jing-hua)